ENVIRONMENTAL RESEARCH
LETTERS

Check for updates

OPEN ACCESS

RECEIVED
26 July 2025

REVISED
18 August 2026

ACCEPTED FOR PUBLICATION
25 August 2026

PUBLISHED
3 September 2026

LETTER

Observation-based mine-level methane emission factors uncover inventory biases and constrain emissions from Shanxi's Coal Mines

Shuhui Fu[1,2], Xin Tong[1], Fei Li[3], Jun Wang[3], Yongguang Zhang[3], Zhaocheng Zeng[4], Zhonghua He[5], Ge Han[6] and Huilin Chen[1,2,*]

[1] Joint International Research Laboratory of Atmospheric and Earth System Sciences, School of Atmospheric Sciences, Nanjing University, Nanjing 210023, People's Republic of China
[2] Frontiers Science Center for Critical Earth Material Cycling, Nanjing University, Nanjing 210023, People's Republic of China
[3] Jiangsu Center for Collaborative Innovation in Geographical Information Resource Development and Application, International Institute for Earth System Sciences, Nanjing University, Nanjing 210023, People's Republic of China
[4] School of Earth and Space Sciences, Institute of Remote Sensing and GIS, Peking University, Beijing 100871, People's Republic of China
[5] Zhejiang Climate Centre, Zhejiang Meteorological Bureau, Hangzhou 310052, People's Republic of China
[6] Hubei Key Laboratory of Quantitative Remote Sensing of Land and Atmosphere, School of Remote Sensing and Information Engineering, Wuhan University, Wuhan 430072, People's Republic of China
[*] Author to whom any correspondence should be addressed.

E-mail: huilin.chen@nju.edu.cn

Keywords: coal mine methane, satellite observations, emission factors, bottom-up inventories, upscaling framework

Supplementary material for this article is available online

Abstract

Bottom-up coal mine methane (CMM) inventories rely on static or empirically derived emission factors (EFs), and therefore mine-level emissions are poorly constrained, limiting the use of these inventories for implementing detailed mitigation strategies. Here, we compiled 1418 satellite-detected methane plumes (2019–2025) and attributed them to 159 active underground coal mines in Shanxi province, China. We further derived observed mine-level EFs, calculated as mine-level emission rates divided by production data. We then compared these observed EFs with those from the State Administration of Coal Mine Safety (SACMS) and Global Coal Mine Tracker (GCMT), and developed a production-capacity-stratified bootstrap framework to upscale emissions from high-gas and outburst coal mines. Observed EFs were highly heterogeneous, right-skewed, temporally variable and negatively correlated with production capacity. Inventory comparisons revealed distinct biases: SACMS reproduced the overall EF magnitude but systematically underestimated EFs for small-capacity coal mines (production capacity <1.2 Mt yr^{-1}), whereas GCMT overestimated EFs for medium- ($1.2\leqslant$ production capacity <3.0 Mt yr^{-1}) and large-capacity coal mines (production capacity $\geqslant 3.0$ Mt yr^{-1}). Using the production-capacity-stratified bootstrap upscaling framework, we estimated 2023 CMM emissions from high-gas and outburst coal mines in Shanxi to be 7.0 [5.6–8.9] Mt yr^{-1}. Total provincial CMM emissions were estimated at 11.2 [9.3–13.6] Mt yr^{-1}. These findings show that satellite-observed plumes can constrain mine-level EFs, reveal inventory biases, and support observation-based provincial CMM estimation.

1. Introduction

Methane is the most important non-CO_2 greenhouse gas in the world (Saunois *et al* 2025). China contributes around half of global coal mine methane (CMM) emissions (Iea 2026). To accelerate CMM emission reductions, China has implemented the 'Methane Emissions Control Action Plan' (Mee 2023). However, mitigation measures ultimately need to be designed and implemented at the coal mine level. Effective CMM mitigation requires not only total emission estimates but also reliable information on how emissions are distributed across individual coal mines.

Bottom-up accounting is commonly used to quantify CMM emissions; however, existing bottom-up inventories in China remain poorly constrained by direct atmospheric observations at the individual coal mine level. In practice, these inventories are built from emission factors (EFs) multiplied by coal production (Ipcc 2006, 2019). In China, bottom-up inventories rely on regional/national default EFs or EFs reported by enterprises (Liu *et al* 2021, 2023, Chen *et al* 2024, Kang *et al* 2024, Khanna *et al* 2024) that lag behind industrial development (Gao *et al* 2021, Liu *et al* 2024, Wang *et al* 2024). However, CMM EFs exhibit significant spatial and temporal heterogeneity, influenced by coal types, mining scales, mining depth, and methane drainage and utilization (Peng *et al* 2023, Rend *et al* 2023, Li *et al* 2025). Without atmospheric observational constraints, these static EFs may misallocate emissions among individual coal mines and mine categories.

Regional top-down estimates can provide important observation-based constraints on total CMM emissions, but they offer limited insight into mine-level emissions or the mechanisms underlying inventory biases (Chen *et al* 2022, Zhang *et al* 2022, Wang *et al* 2025). Their coarse spatial resolution (Shen *et al* 2023, East *et al* 2025) makes it difficult to resolve the contributions of individual coal mines to regional emissions, particularly in coal mining-intensive regions such as Shanxi and Inner Mongolia (Hu *et al* 2024, Tu *et al* 2024). Bridging this gap requires observations that can resolve emissions at the mine level while retaining sufficient spatiotemporal coverage.

Point-source observations provide a promising way: ground-based surveys, uncrewed aerial vehicles-based measurements, and aircraft-based campaigns can localize and quantify emissions at high spatial resolution (Andersen *et al* 2021, 2023, Shi *et al* 2022, Knapp *et al* 2023, Hoerning and Hayes 2025, Penn *et al* 2026), but their limited spatial coverage makes it difficult to characterize emissions across large regions. In contrast, satellite instruments capable of detecting point-source methane emissions (e.g. EMIT, GF-5, PRISMA, EnMAP, ZY1-02D, and GHGSat) can identify methane plumes over much larger areas (Bai *et al* 2024, Han *et al* 2024, Jervis *et al* 2025). By combining mine-level emission rates with production data, these observations can be used to derive observed EFs at the individual coal mine level. However, satellite-observed plumes are instantaneous and detection-limited (Mclinden *et al* 2024), and therefore cannot be assumed to represent all coal mines unconditionally. Inventory evaluation based on such observations therefore requires careful treatment of temporal variability and sample representativeness.

Mine-level inventory evaluation with satellite plume observations requires sufficient plume detections and detailed mine-level data. Shanxi Province provides a suitable testbed for this study because it combines dense distribution of coal mines, detailed mine-level information, and abundant satellite-observed methane plumes. Here, we combine satellite-observed methane plumes with mine-level data to derive mine-level EFs for active coal mines in Shanxi. We characterize the distribution and temporal variability of observed EFs, evaluate the mine-level performance of the State Administration of Coal Mine Safety (SACMS) and Global Coal Mine Tracker (GCMT) inventories, and identify the distinct failure modes of the two inventories. We further develop a production-capacity-stratified bootstrap framework to upscale observed EFs and estimate provincial CMM emissions from high-gas and outburst coal mines. Our results show how satellite-observed methane plumes can be used to characterize mine-level EFs, reveal biases in bottom-up inventories, and support observation-based provincial CMM accounting.

2. Materials and methods

We adopt a three-phase methodological framework: (1) deriving mine-level CMM EFs from satellite-observed methane plumes; (2) evaluating two prior inventories against the observed EFs; (3) estimating provincial CMM emissions from high-gas and outburst coal mines using a production-capacity-stratified bootstrap upscaling framework while propagating uncertainties from observed EFs and activity data. A conceptual workflow is provided in supplementary section S2.

2.1. Derivation of observed EFs

We compiled a dataset of 1418 CMM plume detections spanning 2019–2025 from multi-source satellite observations. The dataset integrates plumes from published studies (Bai *et al* 2024, Han *et al* 2024, He *et al* 2024), non-public plume records provided by GHGSat Inc. (for instrument details, see Jervis *et al* 2021), and the Carbon Mapper Open Data Portal (https://carbonmapper.org/data, Accessed December 2025). For each plume record, we compiled the location, emission rate and its uncertainty, observation date, and satellite source. Adopting the spatial clustering criteria proposed by Jervis *et al* (2025), we clustered individual plumes located within a 2 km proximity into single emission sources. We evaluated the sensitivity to this choice by repeating the plume-clustering, coal mine attribution, mine-level EF calculations, inventory comparisons, and provincial CMM emission point estimation at thresholds of 1–5 km (supplementary section S9). This aggregation mitigates the positional uncertainty in individual satellite plume observations by generating a spatially stable cluster centroid, which we then matched to the nearest registered coal mine. For emission quantification, we pooled all plumes assigned to each cluster across 2019–2025 and used their arithmetic mean emission rate as the cluster-level emission rate. This multi-year mean reduces sensitivity to individual plume events and represents a characteristic detected emission rate over the observation period rather than a year-specific rate. For coal mines associated with multiple clusters, these mean rates were summed to derive the mine-level total methane emission. Figure 1(a) maps the attributed plume clusters and their emission rates. We attributed the methane plumes to 161 distinct coal mines, as shown in figure 1(b). Among them, 159 were active underground coal mines and were classified into low-gas or high-gas and outburst categories according to official gas-level appraisal records (www.chinamine-safety.gov.cn/, Accessed December 2024). We calculated the mine-level observed EF (EF_{obs}, m^3t^{-1}) as follows:

$$EF_{obs} = \frac{\sum_{k=1}^{n} \overline{Q_k} \times 8760}{P \times \rho}$$

where $\overline{Q_k}$ represents the averaged methane emission rate of the *k-th* plume cluster attributed to the coal mine ($kg\,h^{-1}$), and n is the total number of distinct clusters associated with that specific coal mine. P is the annualized coal production capacity ($t\,yr^{-1}$) of the matched coal mine, which was treated as time-invariant over 2019–2025 and used as a proxy for actual annual coal production because mine-level production data are difficult to obtain. The constant 8760 represents the total hours in a year (365 d × 24 h), and ρ is the methane density at 20 °C and 101.325 kPa ($0.67 kg\,m^{-3}$).

2.2. Evaluation of prior inventories

Based on the EF_{obs} of the 159 attributed active underground coal mines, we evaluated two prior emission inventories: EFs derived from underground measurement data compiled by the SACMS in 2011 (Zhang *et al* 2025) and EFs estimated from geological properties in the 2025 release of the GCMT (Global energy monitor 2025). Because annual mine-level EF time series were unavailable for either inventory, we treated them as static benchmarks without temporal adjustment. First, we assessed mine-level agreement between observed and inventory EFs using Spearman's rank correlation coefficient for relative ranking and the coefficient of determination (R^2) from log-log regressions for consistency check. Second, we calculated the geometric mean (GM) of the paired observed-to-prior EF ratios, along with its 95% confidence interval (CI), to quantify the magnitude and direction of the discrepancy. The GM was used because the ratios represent multiplicative differences on a proportional scale and therefore provide a natural measure of the typical relative discrepancy across coal mines. Furthermore, we employed the Wilcoxon signed-rank test to ascertain the statistical significance of the systematic bias. These two analyses were conducted independently on the full sample and across distinct subgroups (coal mine category groups, production capacity classes, and individual coalfields).

2.3. Observation-based provincial emission upscaling framework and uncertainty analysis

Due to known detection limits of satellite observations (Mclinden *et al* 2024, Sherwin *et al* 2024), our observations have a systematic sampling bias for low-gas coal mines. Therefore, we restricted the observation-based provincial emission upscaling to high-gas and outburst coal mines. Given the strong mine-level heterogeneity in observed EFs and their negative correlation with production capacity, this study applied a production capacity stratified bootstrap framework to upscale EFs to all high-gas and outburst coal mines in Shanxi Province. We report the provincial emission estimate for 2023 because both the coal mine list and production capacity data used for upscaling correspond to that year. High-gas and outburst coal mines were divided into 3 production capacity classes based on key Chinese mine-design and capacity-management thresholds: small-capacity coal mines (production capacity <1.20 Mt yr^{-1}), medium-capacity coal mines ($\leqslant 1.2$ production capacity <3.0 Mt yr^{-1}), and large-capacity coal mines (production capacity $\geqslant 3.0$ Mt yr^{-1}).

We estimated provincial high-gas and outburst coal mine emissions using a production-capacity-stratified bootstrap upscaling with 10 000 Monte Carlo iterations. Bootstrap resampling was used to sample EFs from the empirical pool within each production-capacity class, thereby preserving the empirical EF variability in the provincial emission upscaling. The Monte Carlo procedure was used to propagate uncertainty from observed EFs and production to the provincial emission estimate. In each iteration, each target mine was assigned an EF_{obs} that was randomly drawn with replacement from observed mines within the same production capacity class. Following IPCC 2006 guidance, the sampled EF_{obs} was perturbed by drawing from a lognormal distribution whose log-space parameters derived from the observed EF point estimate and its mine-specific standard uncertainty, thereby avoiding physically unrealistic non-positive EF draws. The production capacity of the target mine was independently perturbed using a ±10% triangular distribution to account for potential differences between reported production capacity and actual operating production (Liu *et al* 2024, Wu *et al* 2026). Mine-level emissions were calculated as the product of the perturbed EF and perturbed production capacity, and then summed across all target coal mines. The median and 2.5th–97.5th percentiles of the 10 000 iterations

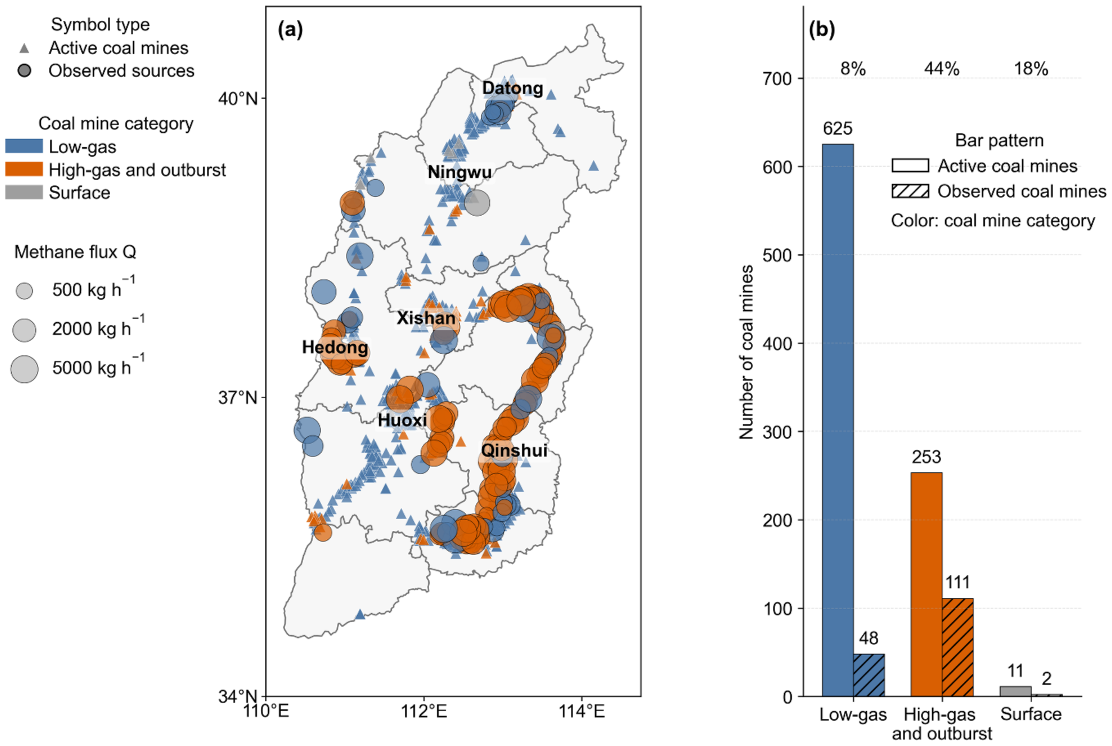

Figure 1. Spatial distribution and observational coverage of coal mine methane sources in Shanxi. (a) Spatial distribution of active coal mines and satellite-observed methane plumes; (b) Comparison between active coal mines and satellite-observed sources by coal mine category.

were reported as the central estimate and 95% uncertainty interval.

The uncertainty in observed EFs was represented by combining uncertainty associated with the satellite-observed emission rates and the production capacity. Uncertainty associated with satellite-observed emission rates included both plume-level emission rate uncertainties and temporal variability inferred from repeated observations, with details provided in supplementary section S3. For high-gas and outburst coal mines with at least three observations and a single plume cluster ($N = 42$), we estimated the absolute temporal uncertainty of EF_{obs} as the standard deviation of repeated emission rates normalized by production capacity. The relative temporal uncertainty was then calculated by dividing this absolute uncertainty by the mine-specific EF_{obs}. For all other coal mines, the median of the above calculated relative temporal uncertainties was multiplied by the mine-specific EF_{obs} to approximate absolute temporal uncertainty. The total uncertainty in EF_{obs} was then estimated by combining these two uncertainty components in quadrature, with details provided in supplementary section S3.

As a sensitivity analysis for high-gas and outburst coal mines, we compared the production-capacity-stratified bootstrap estimate with single-EF estimates using the same provincial production-capacity data. These representative EFs included the arithmetic mean and median of the observed EFs and province-level average EFs from previous studies (Sheng *et al* 2019, Gao *et al* 2021).

3. Results

3.1. Characteristics of observation-based mine-level EFs

Our results show that observed EFs are highly heterogeneous, temporally variable, and partly structured by production capacity. Figure 2(a) shows that the observed EF distributions are right-skewed for both high-gas and outburst and low-gas coal mines. High-gas and outburst coal mines exhibit higher EFs compared to low-gas coal mines, with means of 28.2 ± 31.9 ($N = 111$) and 17.7 ± 15.2 m^3 t^{-1} ($N = 48$), respectively. Both mine categories exhibited substantial mine-to-mine heterogeneity and right-skewed EF distributions, with Fisher-Pearson skewness coefficients of 2.74 and 1.34, respectively. Repeated observations reveal temporal variability in observed mine-level EFs. For high-gas and outburst coal mines with at least three observations and a single plume cluster, the median relative temporal variability of EF_{obs} was 61% (figure S2).

Observed EFs were negatively correlated with production capacity. As shown in figure 2(b), mean EFs were higher for small-capacity coal mines than for

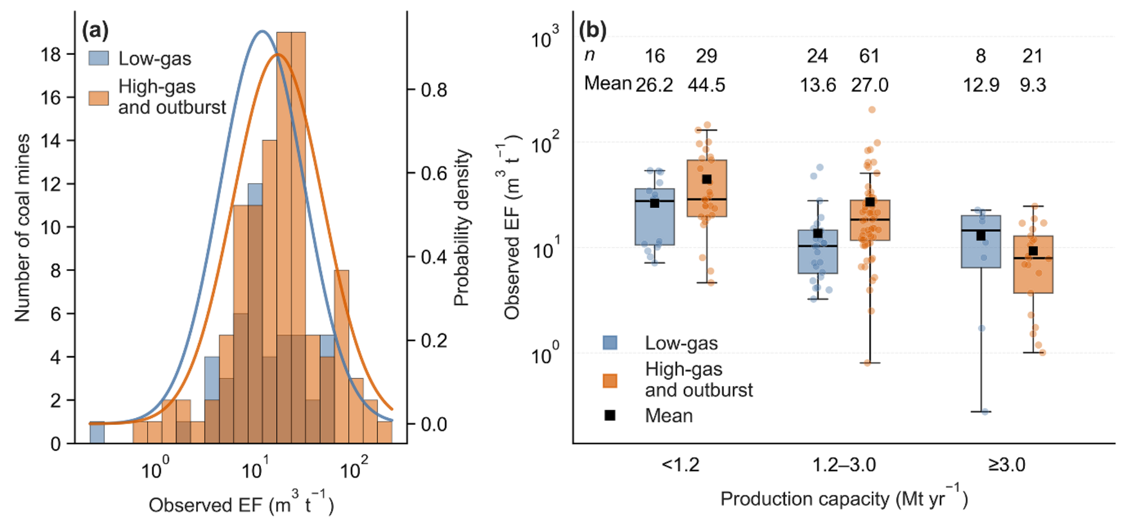

Figure 2. Characteristics of observed active underground coal mine methane EFs in Shanxi. (a) Distribution of observed EFs by coal mine category; (b) Observed EF distributions across production-capacity categories.

medium- and large-capacity coal mines. The log-log relationship between observed EFs and production capacity further supported this dependence, with both high-gas and outburst coal mines ($p < 0.001$; log–log slope $= -0.84$; $R^2 = 0.31$; figure S4) and low-gas coal mines ($p = 0.016$, log–log slope $= -0.75$; $R^2 = 0.26$) showing a negative correlation between EF and production capacity. These slopes imply that a doubling of production capacity was associated with an estimated 44% decrease in EF for high-gas and outburst coal mines and a 41% reduction for low-gas coal mines. This indicates that production capacity partly structures the EF distribution and should be considered when upscaling observed EFs to the provincial coal mines.

The 159 attributed active underground coal mines span all six major coalfields in Shanxi Province, with 117 coal mines located in the Qinshui coalfield, as illustrated in figure 1(a). This spatial clustering likely reflects both dense coal-mining activity and the gas-rich nature of the Qinshui coalfield. This coalfield accounts for approximately 50% of coal mines in Shanxi, and its methane enrichment conditions make it one of China's major coalbed methane basins.

3.2. Limitations of bottom-up inventories

Both SACMS and GCMT inventories show limited ability to reproduce the observed variabilities in mine-level EFs, indicating a common limitation inherent to static inventory methods (figure 3). For SACMS, the log–log relationships between observed and inventory EFs indicated partial explanatory power for both high-gas and outburst coal mines (log–log $R^2 = 0.26$, $N = 58$) and low-gas coal mines (log–log $R^2 = 0.38$, $N = 11$). The overall Spearman correlation ($\rho = 0.44, p < 0.001$) suggests that SACMS retained moderate rank-order information. For the overall sample and gas-level groups, the observed-to-SACMS GM ratios were not statistically different from unity (overall: 95% CI [0.84–1.24]; high-gas and outburst: [0.86–1.27]; low-gas: [0.45–1.80]).

By contrast, GCMT exhibits severely limited coal mine-level predictive capability (high-gas and outburst: log-log $R^2 = 0.05$, $N = 110$; low-gas: log-log $R^2 = 0.00$, $N = 42$). The weak overall Spearman correlation ($\rho = 0.16, p = 0.053$) indicates that GCMT retains little rank-order information at the individual mine level. GCMT exhibits systematic overestimation across the full sample (GM ratio 95% CI: [0.63–0.88], $p < 0.05$). Subgroup analysis reveals that this overestimation is primarily driven by low-gas coal mines (GM ratio 95% CI: [0.39–0.74], $p < 0.05$), whereas the high-gas and outburst coal mines demonstrate no systematic discrepancy GM ratio 95% CI: [0.70–1.02], $p = 0.2$).

SACMS and GCMT exhibit distinct bias patterns across coalfields and production-capacity classes. Spatially, the inventory-matched samples are mainly clustered in the Qinshui coalfield. For SACMS, the coalfield GM ratio approaches 1, indicating broad agreement with observations at the coalfield scale. By contrast, GCMT significantly overestimates EFs in the Qinshui coalfield ($N = 110$, GM ratio $= 0.76$, $p = 0.012$). In the Hedong coalfield, GCMT shows no significant difference from observations ($N = 25$, GM ratio $= 0.97$, $p = 0.98$). Further analysis across production capacity classes reveals that SACMS underestimated EFs for small-capacity class coal mines (GM ratio $= 1.78$, 95%CI: [1.28–2.48], $p = 0.005$). In contrast, GCMT shows no significant bias for small-capacity class coal mines (GM ratio $= 1.15$, $p = 0.40$), but increasingly overestimates EFs with increasing production capacity, particularly for medium-capacity class (GM ratio $= 0.76$, $p = 0.009$) and large-capacity class coal mines (GM ratio $= 0.36$, $p < 0.001$). The opposing production-capacity-dependent bias

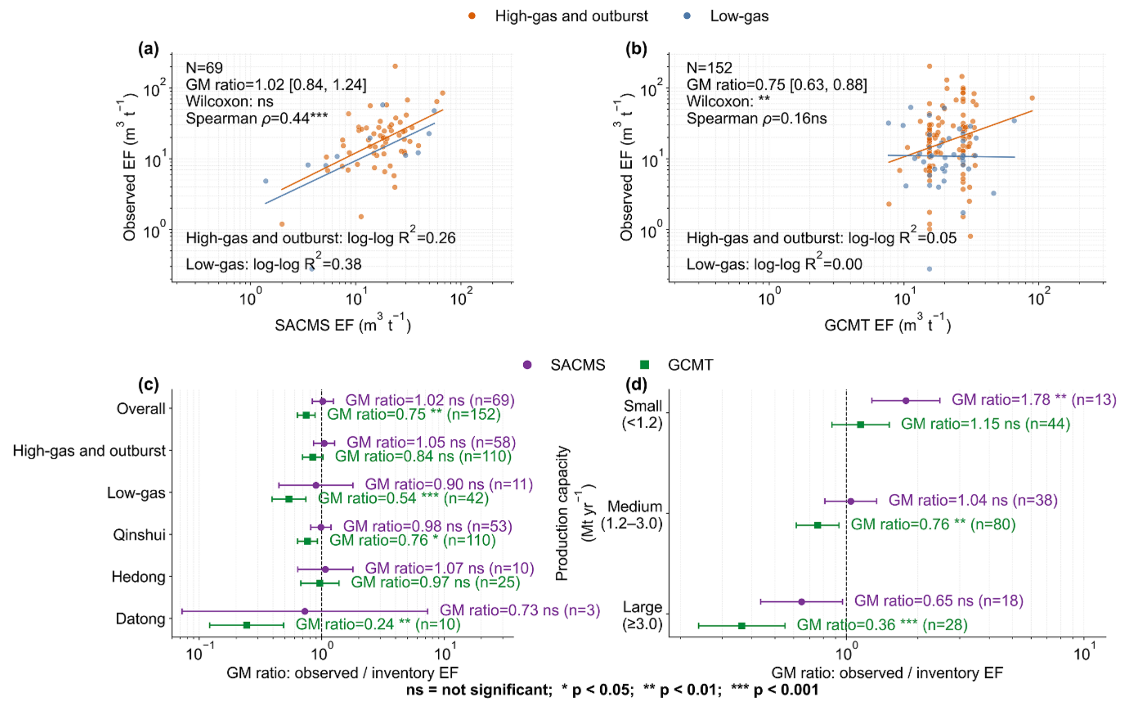

Figure 3. Mine-level comparison of observed and inventory EFs. (a) Observed EF versus SACMS EF;(b) Observed EF versus GCMT EF;(c) Geometric mean ratios of observed to inventory EFs across coal mine categories and coalfields;(d) Geometric mean ratios of observed to inventory EFs across production capacity.

patterns between SACMS and GCMT suggest distinct underlying mechanisms, which are further explored in the Discussion.

3.3. Provincial upscaling of methane emissions from high-gas and outburst coal mines

The right-skewness and production-capacity dependence of observed EFs make provincial emission estimates sensitive to how EFs are treated during upscaling, as illustrated in figure 4(a). The production-capacity-stratified bootstrap upscaling framework yielded a 2023 CMM emission estimate of 7.0 [5.6–8.9] Mt yr^{-1} for high-gas and outburst coal mines. In contrast, applying the arithmetic mean or median of the observed EFs as a single representative value to the same provincial production capacity data yielded emissions of 9.7 and 6.4 Mt yr^{-1}, respectively. This result shows that single representative EFs either overweight or suppress the high-EF tail and cannot preserve the observed EF-production capacity dependence. Estimates based on previous representative EFs also differed, with SACMS-based estimates of 5.7–6.7 Mt yr^{-1}. These lower estimates are consistent with the mine-level finding that previous representative EFs underrepresent the elevated EFs of small-capacity coal mines. Note that only central estimates are compared, as uncertainty ranges were defined differently across studies.

We estimated total CMM emissions in Shanxi Province to be 11.2 [9.3–13.6] Mt yr^{-1} after including emissions from low-gas coal mines, surface coal mines, post-mining activities, and abandoned coal mines (supplementary section S6). High-gas and outburst coal mines had a combined production capacity of approximately 510 Mt yr^{-1}, accounting for approximately 40% of provincial coal production capacity. Yet they contributed approximately 63% of total CMM emissions, making them the dominant source of CMM emissions in Shanxi. As shown in figure 4(b), our total CMM estimate is higher than most previously reported values (6.5–10.2 Mt yr^{-1}; Peng *et al* 2023, Bai *et al* 2024, Chen *et al* 2024, Edgar 2025) but lower than GCMT estimates (15.8–16.8 Mt yr^{-1}). The lower EDGAR estimate may reflect sectoral average EFs that underrepresent the emission intensity of Shanxi's coal mine population or spatial allocation that assigns a smaller share of national emissions to the province. Given differences among studies in year, methodology, and source coverage, this comparison is intended as a contextual benchmark. Our estimate remains within the broader range reported in the literature.

4. Discussion

4.1. Why do SACMS and GCMT differ from observed EFs

SACMS and GCMT adopt different compilation methodologies, leading to persistent discrepancies in their mine-level emission allocations. For instance, while SACMS broadly matched the overall magnitude of observed EFs, our observed EFs for small-capacity

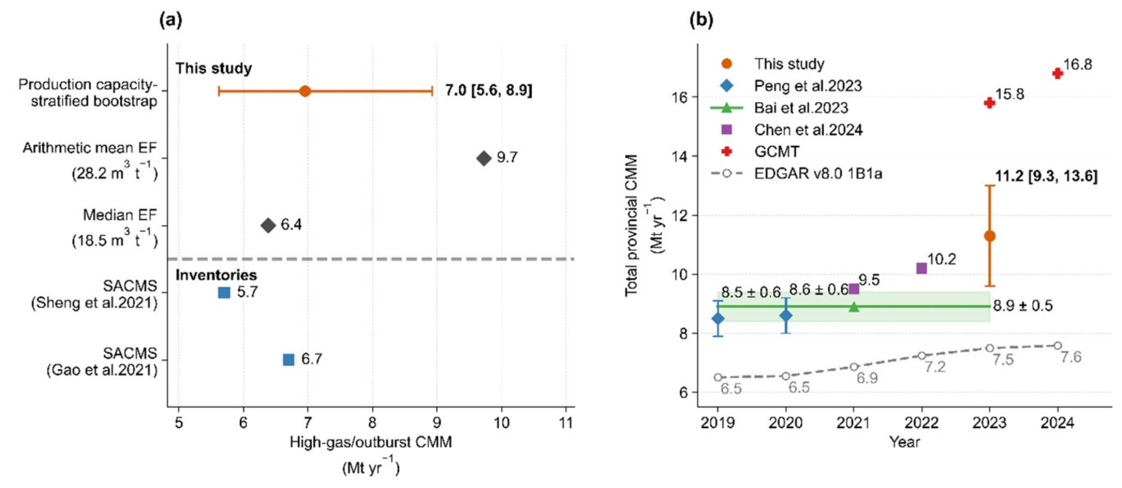

Figure 4. Provincial emission sensitivity to EF treatment and comparison with previous estimates. (a) Provincial CMM for high-gas and outburst coal mines; (b) Total provincial CMM emissions compared with previous studies.

coal mines were 1.78 times higher than SACMS estimates. This systematic underestimation likely reflects both the limited representativeness of short-term gas-level appraisal measurements and differences in operational management.

By contrast, the bias in GCMT is more likely to arise from its simplified treatment of the relationship between emission potential and realized emissions. GCMT estimates EFs primarily from mining depth and the Langmuir adsorption isotherm, thereby approximating methane emission potential rather than the intensity actually emitted to the atmosphere. This method overestimated EFs for medium- and large-capacity mines, with observed-to-GCMT GM ratios of 0.76 and 0.36, possibly because it does not fully account for methane drainage and utilization practices that can reduce actual emissions. The common limitation of both inventories is that they rely on static information, making it difficult to capture temporal variability in EFs driven by engineering and operational factors.

4.2. Geological properties only partly explain observed EF variability

To test whether the static geological properties used by inventories such as GCMT carry predictive signal for observed mine-level EF, we conducted an exploratory random forest analysis (supplementary section S8). The model showed that static geological properties have limited ability to predict mine-level EFs, with a training R^2 of 0.29 and a test R^2 of 0.07. The weak predictive performance suggests that static geological properties alone have limited ability to resolve mine-level EF heterogeneity, which is also shaped by engineering and operational factors. Additional mine-level engineering and operational information is needed to explain the observed EF heterogeneity. To examine how these static geological properties contributed to the exploratory model predictions, we further used SHAP values as a model-interpretation diagnostic. SHAP values quantify whether each predictor shifts the predicted log-transformed EF toward higher or lower values. Gas content showed a threshold-like response in the model, with a transition around 13.5 m^3 t^{-1}. This transition point is close to the critical gas content range estimated from the Langmuir adsorption relationship for Shanxi coal seams, which provides a geological reference for methane occurrence potential and coal-and-gas outburst risk. This consistency suggests that the model response is broadly consistent with known controls on methane occurrence in coal seams. Mining depth and geothermal proxy also influenced model predictions, likely because they partly reflect coal-seam pressure, thermal conditions, and methane retention capacity. Distance to faults contributed in a different way, suggesting that structural conditions may affect methane migration pathways and the spatial redistribution of emissions before they are released through ventilation systems. We emphasize that the random forest model used here represents only one possible approach for exploring the relationship between geological properties and observed EFs, and these findings should therefore be interpreted as exploratory. A comprehensive evaluation of alternative algorithms, feature-engineering strategies, and larger predictor sets is beyond the scope of this study and constitutes a valuable direction for future research.

4.3. Limitations and outlook

The production-capacity-stratified bootstrap upscaling framework provides an observation-based approach for estimating provincial CMM emissions from high-gas and outburst coal mines, making it suitable for handling right-skewed, heterogeneous, and production-capacity-dependent EF distributions. However, the applicability of this framework remains constrained by the representativeness of the observational sample and by plume-to-mine attribution uncertainty. The nearest-neighbor matching approach may misattribute plumes to nearby coal mines. Emissions from low-gas coal mines are often below satellite detection thresholds, leading to limited sample size and detection bias. Therefore, we did not extend the upscaling framework to low-gas coal mines. Even for high-gas and outburst coal mines, satellite observations may be biased toward higher-emitting small-capacity coal mines, potentially biasing observed EFs upward. Moreover, the multi-source satellite datasets used in this study differ in detection thresholds, retrieval algorithms, and other observational characteristics. Such cross-platform differences may affect both the composition of the detected mine sample and the quantification of emission rates, potentially introducing additional uncertainty into the observed distribution of mine-level EFs. Annualizing instantaneous satellite-observed emission rates using 8760 h assumes that the observed emission state is representative of annual average conditions. This assumption may not always hold because emissions can vary with production cycles, methane drainage operations, and intermittent high-emission events. In addition, we assumed a symmetric $\pm$10% triangular distribution to represent uncertainty in reported production capacity, whereas deviations between actual operating production and reported capacity may vary across coal mines. Future integration of higher-precision observations, actual production data, and methane drainage and utilization records would allow this framework to be extended to a broader range of coal mine types and support more complete provincial CMM inventory updates.

5. Conclusions

We compiled and attributed 1418 satellite-observed methane plumes to derive observed mine-level EFs for active underground coal mines ($N = 159$) in Shanxi Province, evaluated these EFs against two bottom-up inventories (SACMS and GCMT), and developed a production-capacity-stratified bootstrap upscaling framework to estimate provincial CMM emissions from high-gas and outburst coal mines. Our study shows that satellite methane plume observations can be translated into mine-level EFs to characterize EF heterogeneity, evaluate static inventory biases and provide an observation-based framework for provincial CMM estimation.

We found that observed EFs are highly heterogeneous, right-skewed, temporally variable, and negatively correlated with production capacity. This production capacity dependence helps explain the biases in bottom-up inventories: SACMS broadly reproduced the overall EF magnitude but underestimated EFs for small-capacity coal mines, whereas GCMT overestimated medium- and large-capacity coal mines. These production-capacity-dependent inventory biases indicate that provincial emission upscaling should preserve observed EF variability across production-capacity classes. Using the production-capacity-stratified bootstrap upscaling framework, we estimated CMM emissions from high-gas and outburst coal mines in Shanxi to be 7.0 [5.6–8.9] Mt yr^{-1}. When other source categories were included, total provincial CMM emissions were estimated to be 11.2 [9.3–13.6] Mt yr^{-1}. However, its application remains constrained by satellite detection thresholds. Extending this framework to broader source categories will require more complete mine-level observations and actual production data to support future CMM inventory updates.

Acknowledgment

This work was supported by the National Key Research and Development Program of China (No. 2024YFB3910201), the Fundamental Research Funds for the Central Universities (No.14380235), and the Fundamental Research Funds for the Central Universities—Cemac 'GeoX' Interdisciplinary Program (2024300245). This research was also supported by the Collaborative Innovation Center of Climate Change, Jiangsu Province.

Data availability statement

The derived mine-level EF dataset and analysis code for mine-level EF calculations, inventory comparisons, provincial emission upscaling, and clustering-threshold sensitivity tests are openly available at: https://doi.org/10.5281/zenodo.21975873. The plume-level inputs used in this study were compiled from multiple third-party sources. Publicly available source materials can be accessed through the original publications and data portals cited in the manuscript.

Supplementary information available at: https://doi.org/10.1088/1748-9326/ae9e4e/data1.

ORCID iDs

Fei Li 0000-0001-9805-9649
Jun Wang 0000-0001-7359-1647
Yongguang Zhang 0000-0001-8286-300X
Zhaocheng Zeng 0000-0002-0008-6508
Ge Han 0000-0003-2561-3244
Huilin Chen 0000-0002-1573-6673

References

Andersen T, Vinkovic K, de Vries M, Kers B, Necki J, Swolkien J, Roiger A, Peters W and Chen H 2021 Quantifying methane emissions from coal mining ventilation shafts using an unmanned aerial vehicle (UAV)-based active aircore system *Atmos. Environ. X* **12** 100135

Andersen T *et al* 2023 Local-to-regional methane emissions from the Upper Silesian Coal Basin (USCB) quantified using UAV-based atmospheric measurements *Atmos. Chem. Phys.* **23** 5191–216

Bai S *et al* 2024 High-resolution satellite estimates of coal mine methane emissions from local to regional scales in Shanxi, China *Sci. Total Environ.* **950** 175446

Chen D *et al* 2024 Characteristics of China's coal mine methane emission sources at national and provincial levels *Environ. Res.* **259** 119549

Chen Z *et al* 2022 Methane emissions from china: a high-resolution inversion of TROPOMI satellite observations *Atmos. Chem. Phys.* **22** 10809–26

East J D *et al* 2025 Worldwide inference of national methane emissions by inversion of satellite observations with UNFCCC prior estimates *Nat. Commun.* **16** 11004

Edgar 2025 Edgar (emissions database for global atmospheric research) community GHG database, version edgar_2025_GHG (European commission, joint research centre (dataset)) (https://doi.org/10.2905/jrc.1k6v990)

Gao J, Guan C, Zhang B and Li K 2021 Decreasing methane emissions from China's coal mining with rebounded coal production *Environ. Res. Lett.* **16** 124037

Global energy monitor 2025 Global coal mine tracker, May 2025 release (dataset) (available at: https://globalenergymonitor.org/projects/global-coal-mine-tracker) (Accessed 25 December 2025)

Han G, Pei Z, Shi T, Mao H, Li S, Mao F, Ma X, Zhang X and Gong W 2024 Unveiling unprecedented methane hotspots in China's leading coal production hub: a satellite mapping revelation *Geophys. Res. Lett.* **51** e2024gl109065

He Z, Gao L, Liang M and Zeng Z-C 2024 A survey of methane point source emissions from coal mines in Shanxi province of China using AHSI on board Gaofen-5B *Atmos. Meas. Tech.* **17** 2937–56

Hoerning S and Hayes P 2025 Measurement of fugitive methane emissions from an abandoned coal exploration hole in Queensland, Australia using a Quantum Gas LiDAR *Sci. Total Environ.* **992** 179925

Hu W, Qin K, Lu F, Li D and Cohen J B 2024 Merging TROPOMI and eddy covariance observations to quantify 5-years of daily CH_4 emissions over coal-mine dominated region *Int. J. Coal Sci. Technol.* **11** 56

Iea 2026 Global methane tracker 2026. Paris: international energy agency (available at: www.iea.org/reports/global-methane-tracker-2026) (Accessed 26 May 2026)

Ipcc 2006 *Ipcc Guidelines for National Greenhouse Gas Inventories* (institute for global environmental strategies)

Ipcc 2019 2019 refinement to the 2006 IPCC guidelines for national greenhouse gas inventories *Volume 2: Energy. Chapter 4: Fugitive Emissions* (Ipcc)

Jervis D *et al* 2025 Global energy sector methane emissions estimated by using facility-level satellite observations *Science* **390** 1151–5

Jervis D, McKeever J, Durak B O A, Sloan J J, Gains D, Varon D J, Ramier A, Strupler M and Tarrant E 2021 The GHGSat-D imaging spectrometer *Atmos. Meas. Tech.* **14** 2127–40

Kang Y, Tian P, Li J, Wang H and Feng K 2024 Methane mitigation potentials and related costs of China's coal mines *Fundam. Res.* **4** 1688–95

Khanna N, Lin J, Liu X and Wang W 2024 An assessment of China's methane mitigation potential and costs and uncertainties through 2060 *Nat. Commun.* **15** 9694

Knapp M, Scheidweiler L, Külheim F, Kleinschek R, Necki J, Jagoda P and Butz A 2023 Spectrometric imaging of sub-hourly methane emission dynamics from coal mine ventilation *Environ. Res. Lett.* **18** 044030

Li X, Cheng T, Zhu H, Ye X, Fan D, Tang T, Tong H, Yin S and Xiong J 2025 High-resolution satellite reveals the methane emissions from China's coal mines *Remote Sens.* **17** 220

Liu G *et al* 2021 Recent slowdown of anthropogenic methane emissions in china driven by stabilized coal production *Environ. Sci. Technol. Lett.* **8** 739–46

Liu Q, Teng F, Nielsen C P, Zhang Y and Wu L 2024 Large methane mitigation potential through prioritized closure of gas-rich coal mines *Nat. Clim. Change* **14** 652–8

Liu S, Liu K, Wang K, Chen X and Wu K 2023 Fossil-fuel and food systems equally dominate anthropogenic methane emissions in China *Environ. Sci. Technol.* **57** 2495–505

Mclinden C A, Griffin D, Davis Z, Hempel C, Smith J, Sioris C, Nassar R, Moeini O, Legault-ouellet E and Malo A 2024 An independent evaluation of GHGSat methane emissions: performance assessment *J. Geophys. Res. Atmos.* **129** e2023jd039906

Mee 2023 Notice on issuing the methane emissions control action plan. Beijing:ministry of ecology and environment of the people's republic of China (available at: https://english.mee.gov.cn/) (Accessed 26 May 2026)

Peng S, Giron C, Liu G, D'aspremont A, Benoit A, Lauvaux T, Lin X, de Almeida Rodrigues H, Saunois M and Ciais P 2023 High-resolution assessment of coal mining methane emissions by satellite in Shanxi, China *Iscience* **26** 108375

Penn E *et al* 2026 Remote sensing enables basin-scale inventories of coal mine methane *Environ. Sci. Technol.* **60** 14924–33

Rend A R, Özer S C, Esen O, Soylu A, Bozdoğan S and Fişne A 2023 Developing basin-specific emission factors for accurate methane inventory and emission reduction strategies in Zonguldak Coal Basin, Turkey: implications for enhancing safety and sustainability *J. Clean. Prod.* **426** 139177

Saunois M *et al* 2025 Global methane budget 2000–2020 *Earth Syst. Sci. Data* **17** 1873–958

Shen L U, Jacob D J, Gautam R, Omara M, Scarpelli T R, Lorente A, Zavala-araiza D, Lu X, Chen Z and Lin J 2023 National quantifications of methane emissions from fuel exploitation using high resolution inversions of satellite observations *Nat. Commun.* **14** 4948

Sheng J, Song S, Zhang Y, Prinn R G and Janssens-maenhout G 2019 Bottom-up estimates of coal mine methane emissions in China: a gridded inventory, emission factors, and trends *Environ. Sci. Technol. Lett.* **6** 473–8

Sherwin E D, El Abbadi S H, Burdeau P M, Zhang Z, Chen Z, Rutherford J S, Chen Y and Brandt A R 2024 Single-blind test of nine methane-sensing satellite systems from three continents *Atmos. Meas. Tech.* **17** 765–82

Shi T, Han Z, Han G, Ma X, Chen H, Andersen T, Mao H, Chen C, Zhang H and Gong W 2022 Retrieving CH_4-emission rates from coal mine ventilation shafts using UAV-based Aircore observations and the genetic algorithm–interior point penalty function (GA–IPPF) model *Atmos. Chem. Phys.* **22** 13881–96

Tu Q, Hase F, Qin K, Cohen J B, Khosrawi F, Zou X, Schneider M and Lu F 2024 Quantifying CH_4 emissions from coal mine aggregation areas in Shanxi, China, using TROPOMI observations and the wind-assigned anomaly method *Atmos. Chem. Phys.* **24** 4875–94

Wang H, Zheng B, Li H, Zhang Q and He K 2024 Targeting ultra-emitters for effective methane mitigation in China's coal sector *Acs es&t air* **1** 734–42

Wang Y *et al* 2025 Towards verifying and improving estimations of china's Co_2 and CH_4 budgets using atmospheric inversions *Natl Sci. Rev.* **12** nwaf090
Wu Z, Wang Y and Teng F 2026 Building a mine-level database of methane emission factors for China's underground coal *Environ. Res. Lett.* **21** 024003
Zhang J, Qiu B, Khanna N and Lin J 2025 Regional production shift and increased utilization dampen the growth of China's coal mine methane emissions *Commun. Earth Environ.* **6** 964
Zhang Y *et al* 2022 Observed changes in China's methane emissions linked to policy drivers *Proc. Natl Acad. Sci. USA* **119** e2202742119